### Title

The Thiol-Rich Interlayer in the Shell/Core Architecture of Mussel Byssal Threads




### Journal

Langmuir, 35(48)

### ISSN

0743-7463



### Authors

Valois, Eric
Hoffman, Carter
Demartini, Daniel G
et al.



### Publication Date

2019-12-03

### DOI

10.1021/acs.langmuir.9b01844

Peer reviewed

LANGMUIR Article
Cite This: Langmuir XXXX, XXX, XXX−XXX
pubs.acs.org/Langmuir

# The Thiol-Rich Interlayer in the Shell/Core Architecture of Mussel Byssal Threads

Eric Valois,[†] Carter Hoffman, Daniel G. Demartini,[†] and J. Herbert Waite[†]

[†]Biomolecular Science and Engineering Graduate Program, University of California, Santa Barbara, California 93106, United States

Supporting Information

**ABSTRACT:** The mussel byssus thread is an extremely tough core-shelled fiber that dissipates substantial amounts of energy during tensile loading. The mechanical performance of the shell is critically reliant on 3,4-dihydroxyphenylalanine's (Dopa) ability to form reversible iron-catecholate complexes at pH 8. However, the formation of these coordinate cross-links is undercut by Dopa's oxidation to Dopa-quinone, a spontaneous process at seawater conditions. The large mechanical mismatch between the cuticle and the core lends itself to further complications. Despite these challenges, the mussel byssus thread performs its tethering function over long periods of time. Here, we address these two major questions: (1) how does the mussel slow/prevent oxidation in the cuticle, and (2) how is the mechanical mismatch at the core/shell interface mitigated? By combining a number of microscopy and spectroscopy techniques we have discerned a previously undescribed layer. Our results indicate this interlayer is thiol rich and thus will be called the thiol-rich interlayer (TRL). We propose the TRL serves as a long-lasting redox reservoir as well as a mechanical barrier.

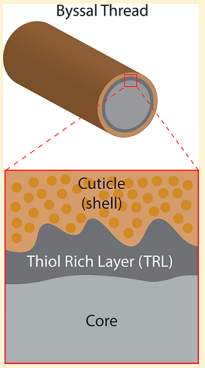


## 1. INTRODUCTION

Materials with core/shell architectures are pervasive throughout nature and technology. Indeed, in nature there may be no functional material without both core and shell. The utility of a core/shell design is self-evident: the core provides bulk properties, e.g., tensile or compressive strength in load bearing materials, while the shell protects the core from corrosion, light, desiccation, microbial attack, and/or abrasion in the ambient environment. Because the disparate functions of shell and core usually lead to incompatibilities between the two, additional adaptive layers are introduced to enhance their union. These are increasingly referred to as self-stratifying coatings[1] and, once again, were evolved by biology, e.g., plant cutins, long before becoming a design concept in engineered materials. Some, but by no means all, biological coatings may thus provide valuable insights for stimulating improvements in manufactured coatings.

Mussel byssal threads have core/shell architectures in which the shell is 5−6 times stiffer than the core.[2] The thread core consists of anisotropic bundles of collagen fibers not unlike tendon,[3,4] whereas the shell, known as the cuticle, is a composite of granules dispersed in a continuous, amorphous matrix. The granules are largely composed of a Dopa-rich mussel foot protein, which, at pH 5−8, readily binds iron to form cross-linking bis- and tris-catecholate-iron complexes.[5,6] Given the reversible nature of metal-coordinate bonds, tris catecholate-iron complexes are reversible sacrificial bonds, dissipating energy by enabling greater strain during deformation. During unloading, the tris-catecholate-iron complexes self-heal to repair damage sustained during deformation but only in a Dopa-rich environment.[8] The high dissolved oxygen content and abundance of trace metals make seawater a powerful oxidant of Dopa[9] thus undermining its integrity in byssal threads, yet Dopa-iron complexes remain stable in the cuticle. How does the mussel protect the cuticle against oxidative damage and consequent loss of function?

Our structural, chemical, and nanomechanical analyses of byssal threads suggest that thread redox is maintained by cuticle stratification in combination with thiol enrichment in a subsurface layer, i.e., the thiol rich layer (TRL). A combination of microscopy techniques including transmission electron microscopy (TEM), scanning electron microscopy (SEM), and atomic force microscopy were used to characterize the location and morphology of this TRL. Furthermore, fluorescence microscopy, X-ray near edge spectroscopy (XANES), and secondary ion mass spectrometry were used to speciate the thiol.

Prior studies have identified the cuticle as being significantly stiffer than the core.[7] While this unique combination of stiff cuticle and compliant core results in high toughness, it creates the possibility of contact damage at the interface between the two mechanically mismatched materials. Here, we characterize the nanomechanical characteristics under biologically relevant conditions using indentation type atomic force microscopy. Although our measurements confirm a large discrepancy in elastic modulus between cuticle and core, they also reveal that the inclusion of the TRL creates a step gradient in hardness and abrasion resistance. By building on many years of byssus research, the present study addresses two major gaps in our understanding. First, how the cuticle copes with an oxidizing

**Special Issue:** Intermolecular Forces and Interfacial Science

**Received:** June 17, 2019
**Revised:** August 12, 2019
**Published:** August 12, 2019






DOI: 10.1021/acs.langmuir.9b01844
Langmuir XXXX, XXX, XXX−XXX

environment, and second, how the byssus successfully joins two mechanically mismatched materials.

## 2. RESULTS

**Ultrastructural Characterization of Distal Byssus.** Transverse cross-sections of distal byssal threads from local *Mytilus californianus* reveal the three distinct regions: (1) cuticle, (2) TRL, and (3) core. The granular structure of the cuticle is readily visible with TEM and is characterized by the presence of ∼500 nm (diameter) electro-lucent granules surrounded by an electron-dense protein matrix at a fill ratio of 1:1 (Figure 1B).[10] Granules are the primary location of iron-catecholate complexes in the byssal thread[6] and function to increase the abrasion resistance of the exterior coating and prevent dehydration during times of exposure to atmosphere.[3,4,10] The core of each byssal thread consists of anisotropic microbundles of collagen fiber bundles oriented parallel to the long axis of the thread (Figure 1C–E). In this study, high resolution transmission electronmicroscopy (STEM) was employed to measure an average diameter of 13.6 ± 1 nm (S1).

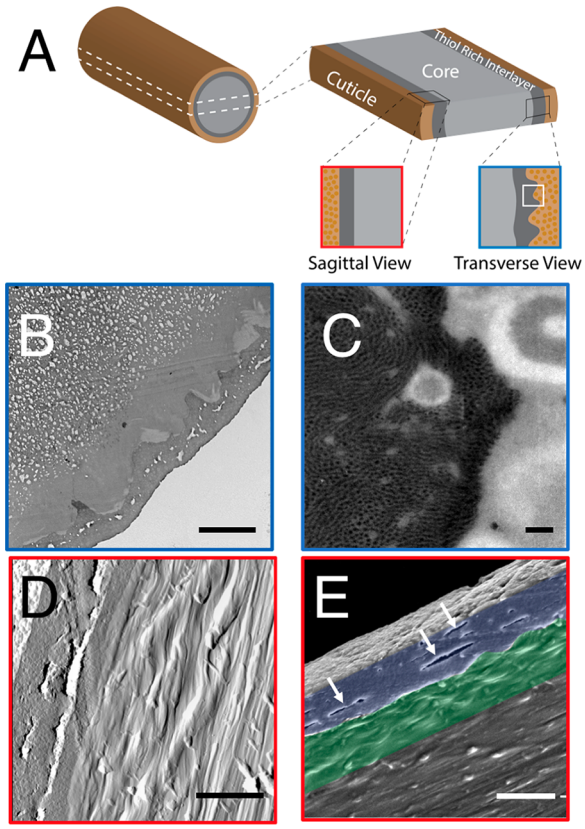


**Figure 1.** Byssal thread cross-sections. Parts B and C are transverse cross-sections. Parts D and E are sagittal cross-sections. (A) Illustration of mussel byssal thread components and location. (B) Transmission electron micrograph of transverse section of mussel byssus thread in which the cuticle, TRL, and core are visible moving from bottom to top. Scale bar is 5 μm. (C) Zoom of TRL as observed in STEM. The epresentative region of part C is shown by white box in part A. Scale bar is 100 nm. (D) AFM amplitude image of a sagittal section of the byssal thread. Moving from left to right, the cuticle, TRL, and core are all visible. Scale bar is 5 μm. (E) SEM of the byssal thread section. Visible are circumferential cracks/voids in the cuticle (white arrows), the "wavy" interphase (green), and fibrous core (black). Scale bar is 5 μm.

Sandwiched between the cuticle and core, an electron dense homogeneous material is discernible. We shall refer to this as the thiol rich layer (TRL). However, as revealed by STEM, true homogeneity is complicated by interfacial penetration of TRL by collagen fibers (Figure 1C). Fibers within the TRL maintain a diameter similar to that of the core, 13.6 ± 0.7 nm (S1). Furthermore, fibrillar center to center distance, indicative of collagen packing density, remains unchanged; 22.3 and 23.7 nm for the TRL and core, respectively. We interpret this to mean that collagen in the TRL is not significantly different from that of the core.

In thin (<100 nm) transverse sections, collagen bundles contained in the TRL appeared to maintain their anisotropy. However, imaging of sagittal cross-sections demonstrated that fibers in the TRL were more isotropic (Figure 1D). Furthermore, voids and cracks that formed in the cuticle as the result of normal deformation became visible. Interestingly, these cracks were deflected by the TRL and were only propagated parallel to the long axis of the fibers (Figure 1E).

**Biochemical Characterization.** The byssal thread is formed by a processive injection molding of secretory vesicles from two specific glands in the ventral groove of the foot.[11] The collagen gland contains prolate ellipsoid vesicles containing collagen mesophases, which self-assemble into mature collagen fibers during molding of the core (Figures 2A and S2). The coating or cuticle is formed when the accessory gland secretes spherical vesicles with a "marbled" internal structure[11] that flow over and coat the nascent collagen core. Recently, in-depth analysis of the accessory gland transcriptome revealed, at the mRNA level, the presence of four novel mussel foot proteins (mfps); mfp-16, -17, -18, -19. This cohort of mfps contained cysteine levels ranging from 7 to 20 mol percent.[12] By isolating cuticle and collagen vesicles from their respective glands, we directly confirmed one of the aforementioned proteins (Figure 2B). A dispersion of granules prepared from the accessory gland was trypsinized and subjected to ESI-TOF-MSMS. A positive identification of the sequence HDDYSSDPYTEPQK was made to residues 85–99 of a 21 kDa protein, mfp-17.[12] The full cysteine-enriched sequence is shown in Figure 2C. Sequences for other proteins known to exist in the isolated secretory vesicles, namely, preCol-D and preCol-NG, are shown in Supporting Information, Figures S6 and S7, respectively.

Thin (10 μm) transverse sections were incubated with Alexafluor 555 $C_2$ Maleimide, a cysteine specific fluorescent reporter, and subjected to confocal fluorescent microscopy. When illuminated with 550 nm light, the ∼5 μm region identified as the TRL fluoresced (Figures 3B and S3) and agreed with an earlier detection of sulfur enrichment by electron dispersive X-ray spectroscopy.[13] While the core exhibits small degrees of fluorescence, attributed to a single cysteine residue in each preCol-D chain, the intensity in the TRL is 250% higher (Figure 3D). Thiol-maleimide Michael addition is necessarily dependent upon thiolate formation under pH conditions at or above the thiol p$K_a$, typically >7. Accordingly, the evolution of fluorescence in the TRL suggests that prior to maleimide addition, cysteine side chains are not engaged as disulfides. To confirm the presence of cysteine, not cystine, micro-X-ray absorption near edge spectroscopy (μXANES) at the sulfur K edge was conducted. Sulfur XANES is a powerful tool for chemical characterization in


DOI: 10.1021/acs.langmuir.9b01844
Langmuir XXXX, XXX, XXX−XXX

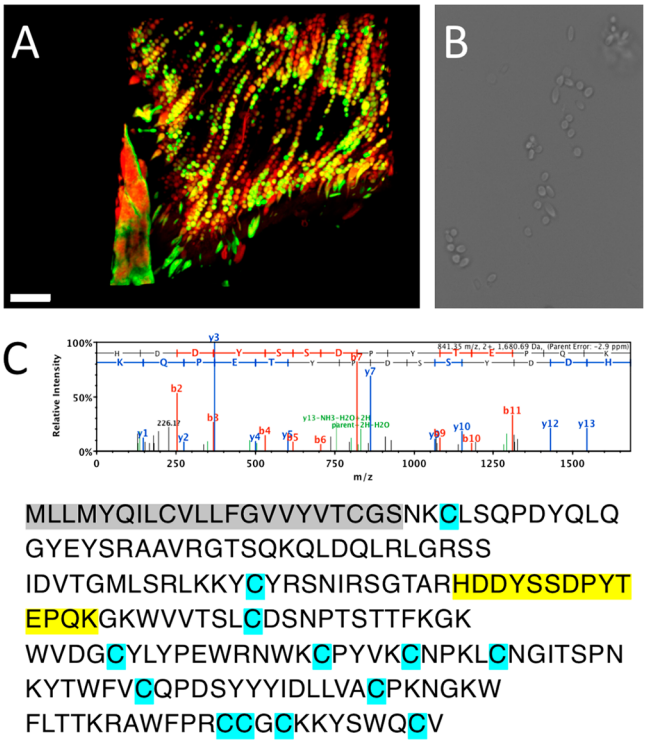


**Figure 2.** Secretory vesicles packed with byssal precursors in accessory gland cells of the mussel foot. (A) Fluorescent micrograph of secretory granules in the foot. Scale bar is 100 $\mu$m (B) Optical micrograph of granules isolated from the foot by differential centrifugation. Circular granules contain cuticle precursors and are stored in the accessory gland. Prolate vesicles contain pre-Col. (C) Lower panel: complete sequence of mfp-17 with the yellow highlight being positively identified via tandem mass spectrometry. Upper panel: MSMS spectra used for identification.

complex biological systems and is particularly well suited for the determination of sulfur speciation due to large chemical shift ranges and sharp line widths.[14] The TRL has an absorption maximum centered at 2473.59 eV, characteristic of sulfur with a −2 oxidation number[15] and consistent only with reduced thiols (Figure 3E).

Surprisingly, the cuticle exhibited no signs of cysteine in either fluorescence microscopy (FM) or XANES. Because the oxidation state of sulfur has a profound effect on detection by both techniques, it was important to verify the results with a third technique that is independent of oxidation state. Secondary ion mass spectrometry (SIMS) provides element specific mapping at 1 $\mu$m resolution with sensitivity in the singles of ppb but, most importantly, is unaffected by oxidation state.[16] By bombarding a thread section with $^{133}Cs^{+}$, the generation of $^{32}S^{-}$ was monitored and mapped to the sample surface. In concurrence with FM and XANES, sulfur levels in the cuticle were below the detectable limit (S4).

**Reducing Capability.** The average standard redox potential of $O_2$ in seawater is ~600 mV SHE, substantially higher than that of DOPA contained in mfps,[17] making the coupling of oxygen reduction with DOPA oxidation a likely event. DOPA oxidation to DOP Aquinone compromises its ability to form the metal coordinate complexes, which are essential to the cuticle's cohesion and self-healing behaviors.[2,18,19] The high cysteine density of the TRL provides the cuticle with a dedicated redox reservoir which can be called upon in times of increased oxidative stress. The antioxidant capacity of the byssal thread was probed using the redox dye 2,2-diphenyl-1-picrylhydrazyl (DPPH). DPPH absorbs maximally at 517 nm in its oxidized form;[20,21] however, bleaching occurs when it is exposed to a reducing agent such as cysteine. Incubation of byssal thread cross-sections with DPPH reveals a sustained antioxidant capacity ($t_{1/2}$ ~ 100 min) (Figure 4). By comparison, free cysteine lost 50% of its reducing capacity in <5 min. To demonstrate that cysteine side chains in thread proteins are the primary source of reducing equivalents, thread cross-sections were treated with iodoacetamide (IAM) prior to the DPPH assay. IAM modification of cysteinyl-thiol produces cysteine-*S*-acetamide, which is incapable of DPPH reduction. The resulting assay yielded a less than 3% decrease in DPPH absorption over 60 min, confirming that thiols are the major primary reductant in the thread.

**Mechanics.** Position-specific mechanics were probed using indentation type atomic force microscopy (IT-AFM). IT-AFM provides two key advantages compared with other mechanical testing methods. (1) By overlaying topology imaging with force-spectroscopy mapping (FM) one can obtain location specific mechanics with a spatial resolution approaching 10 nm[2]. (2) The sample testing environment can easily be changed without removing the sample. This is of particular interest to the mussel thread which experiences both wet and dry conditions in nature. This study is the first to probe location specific nano-mechanics while being submerged in seawater.

In IT-AFM, the probe is rastered across a previously generated topology image, generating a force vs displacement curve at each pixel. The result is a 2D array of force vs displacement curves (FM) from which the modulus and hardness at each pixel are extracted. Under dry conditions, force-spectroscopy maps reveal a shallow gradient of increasing stiffness from the core (1.05 GPa n = 1298) to the TRL (1.12 GPa n = 1298) to the cuticle (1.28 GPa n = 1040) (Figure 5A).

By switching the testing environment from dry to submerged, dramatically different mechanical behavior emerges. When submerged in seawater, the cuticle stiffness decreases 2.25-fold to ~550 ± 106 MPa. Once hydrated, theTRL and core soften 25- to 50-fold to 45 ± 7 and 20 ± 5 MPa, respectively (Figures 5A and S5).

Functional gradients are designed to create high-performance materials by confining and insulating specific compositions and architectures to regions of need.[22] As is the case with most core/shelled fibers, the shell is usually designated as a protective outer coating. Consistent with this, the mussel cuticle's stiff granular structure has a hardness ($H$) of 220 ± 60 MPa (Figure 5B). Using Ashby plots of critical properties, the abrasion resistance of a material can be comparatively assessed by plotting $H$ vs $E$. Materials which fall on a straight line of slope 2/3 have equivalent performance and can be grouped according to their $H^3/E^2$,[23]. The cuticle "$H$' and '$E$" yield a $H^3/E^2$ of 35 MPa, putting it in the realm of most engineering epoxies. In the TRL, both $E$ and $H$ decrease by an order of magnitude to 26 ± 10 MPa. However, the resulting $H^3/E^2$ is 9 MPa, only a 4-fold decrease from the cuticle. Given that the core's primary function is to dissipate tensile energy, the need for hardness is not readily apparent. Fittingly, the measured hardness of the core is 9 MPa, with a $H^3/E^2$ of 1.5 MPa.



DOI: 10.1021/acs.langmuir.9b01844
*Langmuir* XXXX, XXX, XXX−XXX

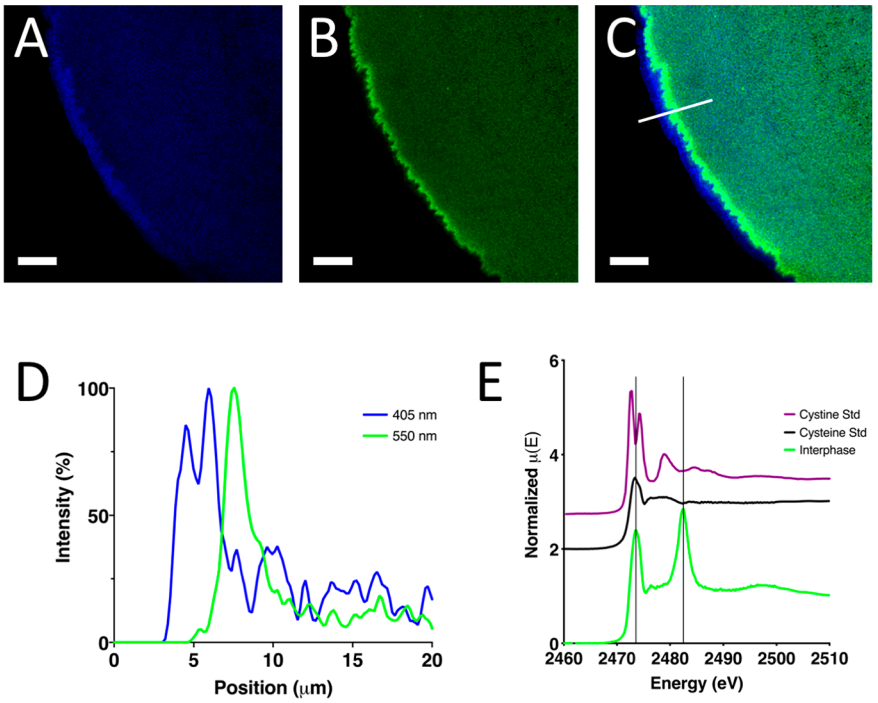


**Figure 3.** Localization of cysteine residues in the thread. (Parts A–C) Fluorescent micrographs of transverse cross-sections at varying excitation wavelengths. (A) Excitation at 405 nm used to visualize the cuticle. (B) Excitation at 550 nm. (C) Overlay of A and B. Scale bars in A–C are 10 $\mu$m (D) Intensity profile of fluorescence from white line in part C. (E) XANES spectra of the interphase (green) vs cysteine (black) and cystine (purple) standards.

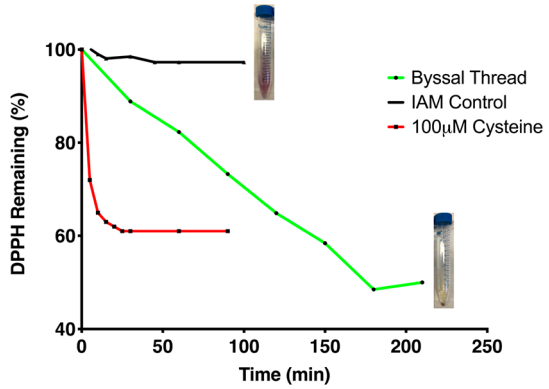


**Figure 4.** DPPH Assay. Sustained redox activity is observed in byssal threads (green) whereas the cysteine control quickly reduces the DPPH (red). When treated with iodoacetamide (IAM) to block cysteine and prevent DPPH reduction, no change is observed in oxidized DPPH levels (black).

## 3. CONCLUSION

Prior studies have classified the byssal thread as a coated, fiber-filled composite material with distinct shell and core domains. By combining microscopy, spectroscopy, and mechanical analysis techniques we introduce a third, multifunctional thiol rich layer. The TRL is an approximately 5 $\mu$m thick region intercalated between the cuticle and core and is characterized by an increase in cysteine density compared with the two adjoining domains. Additionally, we show that cysteine residues in the TRL persist in their reduced state. Cysteine clustering has been shown in a number of proteins and often increases in proteins designed to deal with high oxidative stress,[24] such as that experienced by the byssus. Given that the mechanical performance of the cuticle necessarily relies on Dopa's ability to form tris-Dopa-iron complexes, which deteriorate upon Dopa oxidization, we propose that the TRL provides a reservoir of electrons to create a sustained reducing environment to protect the cuticle against oxidative damage. Despite being submerged in seawater for 24–48 h, the threads used for these studies indicated no cysteine oxidation. Further studies to investigate the aging process of the TRL are underway. Given its thiol rich nature, the formation of a variety of covalent bonds including disulfide and cysteinyl-dopa[25] adducts are possible over time. The penetration of collagen fibers into this dense thiol-rich matrix creates a mechanically distinct barrier between the cuticle and the core. The inclusion of this interlayer forms a step gradient in hardness and abrasion resistance from the cuticle to the core which helps mitigate contact damage. Furthermore, composite structures of stiff outer materials underlaid by a gradient of compliant materials favor superficial circumferential cracking as opposed to deep penetrating radial cracking.[22] The prevention of radial cracking prevents cracks from entering the core, which would result in catastrophic failure under tension. The multifunctionality of the TRL addresses two major problem areas of the mussel byssus; oxidation and mechanical mismatch. By further understanding the role of redox chemistry at biological interfaces, we gained valuable knowledge, which may lead to smart design principles for layered load bearing materials.

## 4. MATERIALS AND METHODS

**TEM/STEM.** Threads less than 48 h old were excised from the animal and fixed according to the following procedure: all fixation and washing steps were performed on ice. Threads were fixed with 2% formaldehyde and 2.5% glutaraldehyde in fixation buffer (200 mM sodium cacodylate, 300 mM NaCl, pH 7.2) for 2 h. The samples were washed three times (10 min each) in degassed fixation buffer and then postfixed in 2% osmium tetroxide in degassed fixation buffer for 2 h.



DOI: 10.1021/acs.langmuir.9b01844
Langmuir XXXX, XXX, XXX–XXX

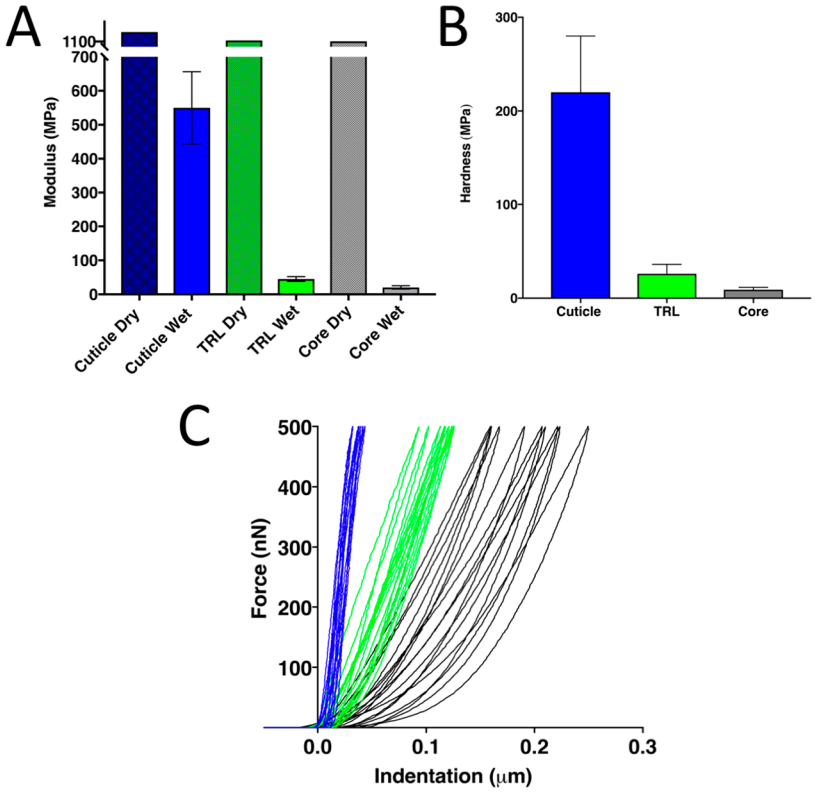


**Figure 5.** Location specific mechanics as measure by indentation-type atomic force microscopy. (A) Elastic modulus of the cuticle, TRL, and core under wet and dry conditions. (B) Hardness values extracted from force vs indentation profiles from submerged samples shown in part C. (C) 10 representative F vs I profiles from each hydrated region. Cuticle (blue), TRL (green), core (black).

The samples were then washed four times (10 min each) in degassed deionized water and then dehydrated through a graded series of ethanol washes (25, 50, 75, 90, 100, 100, 100% ethanol, 10 min each). Solvent was then switched to propylene oxide by washing in 33, 66, 100, 100, 100% propylene oxide in ethanol. The samples were then infiltrated with epoxy resin (Embed812, Electron Microscopy Sciences, Hatfield, U.S.A.) by incubating the sample in resin that was diluted in propylene oxide as follows: 33% (2 h), 66% (16 h), and 100% (4 h). Finally, samples were placed in molds and cured at 60 °C for 24 h. Thin sections (60−80 nm) for TEM were cut on an EM UC6 ultramicrotome (Leica Biosystems). Sections were mounted on copper TEM grids and poststained on drops of uranyl acetate and lead citrate following standard protocols. All samples were investigated with a Tecnai G2 transmission electron microscope (FEI) operating at 200 kV, and micrographs were recorded with a GatanUltrascan CCD camera (2048 × 2048 pixels. STEM images were acquired using a Titan transmission electron microscope operating at 300 kV. Collagen spacing was calculated using Fiji's (v. 2.0.0-rc-65) nearest neighbor distance (NND) plugin. Prior to analysis, each image was smoothed, and a threshold was applied resulting in a binary image.

**Atomic Force Microscopy (AFM).** Images and force measurements were conducted on a MFP-3D Bio (Asylum Research, Santa Barbara, CA). FORTA silicon tips (APPNano, Mountain View, CA) were used in all experiments. Fresh threads (<48 h old) were imbedded in Neg-50 cryoprotectant (Rachard-Allan Scientific, San Diego, CA) and frozen to −20 °C. Ten micrometer thick sagittal sections were cut using a Leica Cryostat. Sections were placed on top of a drop of water on a poly lysine slide. The water was subsequently removed with a gel loading pipet tip causing the section to lie flat on the slide. Once mounted, sections were allowed to dry for 1 h prior to measurement, ensuring sufficient adherence to the slide. Topology images (20 $\mu m^2$) were generated using AC mode at a rate of 0.7 HZ. For submerged samples, threads were allowed to equilibrate in seawater for 1 h prior to imaging. Prior to force measurements, the cantilever spring constant was experimentally determined by the thermal tune method usually ranging between 2 and 3 N/m. Deflection sensitivity was calculated using a glass slide as an indefinitely stiff calibrant material. Force spectroscopic maps of 32 × 32 pixels were recorded over previously acquired topology images. Force spectroscopy measurements were conducted at 250 nm/s load/unload rate with a maximal loading force of 500 nN. Stiffness and hardness values were calculated by Asylum Research's Elastic Analysis Tool by fitting the upper 1/3 of the loading curve, an indenter half angle of 20°, and a Poisson ratio of 0.33 to the Hertz Model.

**SEM.** Fresh threads were fixed with 2% formaldehyde and 2.5% glutaraldehyde in fixation buffer (200 mM sodium cacodylate, 300 mM NaCl, pH 7.2) for 2 h. Fixed threads were imbedded in Neg-50 cryoprotectant (Rachard-Allan Scientific, San Diego, CA) and frozen to −20 °C. Ten micrometer thick sagittal sections were cut using a Leica Cryostat. Sections were washed three times for 10 min each in milli-Q water to remove any excess cryoprotectant. Solvent exchange from water to ethanol was performed in steps of 30%, 50%, 60%, 90%, 100% X3 ethanol. Samples were dried and secured to an aluminum imaging stub with double sided carbon tape. A thin layer of gold/palladium (60:40) was sputter-coated onto the sample for 100 s using anAnatech USA Hummer 6.2 coater. Specimens were viewed at 3 kV with a FEI Nova Nano 650 FEG SEM.

**Fluorescence Microscopy.** Transverse cross-sections of fresh mussel threads were prepared as described above. Sections were washed three times (1 min each) to remove excess cryoprotectant followed by three times (5 min each) of washing in phosphate buffered saline (PBS) pH 7.4 (Gibco Life Technologies). Washed sections were incubated in 1 $\mu$M Alexa Fluor$_{555}$ $C_2$ Maleimide (Thermo Fisher Scientific, Waltham, MA) in PBS for hours at room temperature. Alexa Fluor 555 $C_2$ Maleimide stock was prepared by dissolving the received product in dimethyl sulfoxide to a final concentration of 10 mM. Following staining, sections were rinsed three times (10 min each) in PBS to remove excess dye and subsequently mounted onto glass slides using ProLong Gold Antifade


DOI: 10.1021/acs.langmuir.9b01844
*Langmuir* XXXX, XXX, XXX−XXX

Mountant (Thermo Fisher Scientific, Waltham, MA). Confocal images were collected using a Leica SP8 confocal microscope (Leica Microsystems) fitted with 63X/1.4NA oil immersion objective and hybrid detectors (HyD). Thread cuticle was visualized via its intrinsic fluorescence when excited with a 405 nm laser. Alexa Fluor$_{555}$ stained TRL was visualized using the white light laser tuned to 550 nm excitation. Comparative fluorescent intensity was calculated with Fiji's analyze plot profile function. Alkylation of cysteine residues was accomplished using iodoacetamide (IAM). In control threads, alkylation was done prior to Alexa Fluor$_{555}$ $C_2$ Maleimide addition by incubating thread sections in 60 $\mu$M IAM in PBS (pH 7.4) for 1 h.

**Accessory and Collagen Granule Isolation and Tandem MS.** Live *Mytilus californianus* were collected from the Goleta Pier in Goleta, CA and stored in maricultural tanks with an open seawater circulation system. Feet were excised from the mussel and sliced into sections approximately 3 mm in length using a no. 10 scalpel. The distal portion of the foot surrounding the distal depression was discarded in order to avoid contamination from phenol gland granules. Gland tissue at the center of the foot was carefully separated from the pigmented epithelium and homogenized in 1 mL per foot of 0.05 M sodium phosphate (pH 7.4) with 0.45 M NaCl (mPBS). Granules were separated from insoluble tissue by successive centrifugation through a 40 $\mu$m mesh followed by 5 $\mu$m mesh (2× for 10 min each at 500g). If necessary, additional mPBS was used to rinse the mesh in between spin cycles to prevent clogging. After the final centrifugation, granules were pelleted at 1000 *g* for 10 min and the supernatant was removed. Pelleted granules were resuspended in 0.1 M citrate (pH 5.0) with 0.6 M sucrose, 0.005 M ascorbic acid, and 0.001 M EDTA. Resuspended granules were then subjected to a differential centrifugation gradient of 10 to 50% OptiPrep (Alere Technologies, Waltham, MA) for 16 h at 31000 rpm, 4 °C (Beckman L8-80 M Ultracentrifuge, Beckman Coulter, Brea, CA). Granules contained in 40% Optiprep were collected for trypsinization. Optiprep was removed from the sample by dilution at 1:10 with mPBS and repelleted at 1000 *g* for 5 min × 3. Trpysinization was done in 50 mM Tris-HCl (pH 8), 5 mM DTT, and 8 M urea at 37 °C for 4 h. Resulting peptides were sent to the UC Davis mass spectrometry facility for sequencing (Davis, CA). Peptides were quantified, and 1.0 $\mu$g was injected into the Xevo G2 QT mass spectrometer coupled to a nano-UPLC system (Waters, Milford, MA. U.S.A.). Peptides were injected into a nanoTile, housing a C18 column, and were eluted off the column in a 1 h gradient from 2 to 60% acetonitrile. Mass spectrometry analysis was done using MSe, a data independent acquisition (DIA) method. Data analysis was done using a Protein Lynx Global Server, and the data was subsequently analyzed in Scaffold-4 (Proteome Software, Portland, OR, U.S.A.)

**$\mu$XANES.** To determine in situ sulfur species, synchrotron-based sulfur X-ray absorption near-edge spectroscopic (S XANES) measurements were made at the beamline (BL) 14−3 at the Stanford Synchrotron Radiation Lightsource (SSRL) using a Si(111) ($\Phi$ = 90) double crystal monochromator. The monochromator was calibrated at the thiol pre-edge energy of a sodium thiosulfate powder to 2472.02 eV. The fluorescence lines of interest were measured with a Si Vortex Si drift detector (SII Nano Technology) using Xspress3 pulse processing electronics (Quantum Detectors) that deliver superior count rates without significant dead times. The X-ray beam was focused using Kirkpatrick-Baez (K−B) mirrors to a size of ~3 × 3 $\mu$m at a flux of ~2 × 1010 photons per second. To determine sulfur speciation at specific points within the sample, absorption spectra (S XANES) were collected from 2460 to 2536 at 0.2 eV steps to capture the range of energies for the absorption edges of possible common sulfur compounds. Multiple spectra were acquired at each point to confirm that the absorption edge energies did not shift to lower energies because of photoreduction by beam damage to the sample.

**SIMS.** Sagittal sections of threads less than 48 h old were excised from the animal and prepared according to TEM procedures. Thin sections were then mounted to a silicon wafer. To ensure a flat sample surface, sections were floated on a small drop of water placed on top of a silicon wafer. The water droplet was slowly evaporated by heating the wafer to 50 °C with a heating block. Elemental mapping was conducted using a Cameca IMS 7f-Auto SIMS. Negative ions ($^{32}S^-$ and $^{26}CN^-$) were mapped with a primary cesium gun using 15 kV of impact energy and a spot size of 1.5 $\mu$m.

**DPPH Assay.** Given the light sensitivity of DPPH, all reaction vessels containing DPPH were wrapped in foil. A 2 mM stock solution was made by resuspending DPPH in 99.5% ethanol. A 100 $\mu$L portion of stock was added to 900 $\mu$L of ethanol. The resulting 0.2 mM DPPH solution was mixed 1:1 with 0.1 M Tris buffer (pH 7.4). A 5 mg portion of sectioned threads was added to the solution and mixed by tube inversion. The absorbance at 517 nm was monitored over time. A blank solution was prepared by replacing 100 $\mu$L of stock with 100 $\mu$L of ethanol. As a control, 100 $\mu$L of stock was replaced with 100 $\mu$M cysteine. The percentage of DPPH remaining was calculated by the following equation

$$\% \text{ remaining} = (\text{Abs}_{\text{sample,t}}/\text{Abs}_{\text{control,t}} \times 100)$$

## ■ ASSOCIATED CONTENT

### Supporting Information

The Supporting Information is available free of charge on the ACS Publications website at DOI: 10.1021/acs.langmuir.9b01844.

STEM images used for collagen bundle size and spacing calculation, localization of secretory granules in the foot of *M. californianus*, fluorescent micrographs of transverse cross-sections, secondary ion mass spectrometry images, comparison of wet and dry AFM images of byssal threads, partial sequences of preCol-D tryptic peptide and preCol-NG tryptic peptide via CID tandem mass spectrometry (PDF)

## ■ AUTHOR INFORMATION


### ORCID

Eric Valois: 0000-0002-6824-2933


### Author Contributions

E.V. and J.H.W. conceived the research and wrote the manuscript. E.V., C.H., and D.G.M. planned and performed all experiments. All authors contributed revisions to the manuscript.


### Funding

This research was supported by the Materials Research Science and Engineering Centers Program of the National Science Foundation under award DMR 1720256. We acknowledge the use of the NRI-MCDB Microscopy Facility and the Resonant Scanning Confocal supported by NSF MRI grant 1625770


### Notes

The authors declare no competing financial interest.

## ■ REFERENCES


(1) Beaugendre, A.; Degoutin, S.; Bellayer, S.; Pierlot, C.; Duquesne, S.; Casetta, M.; Jimenez, M. Self-Stratifying Coatings: a Review. *Prog. Org. Coat.* **2017**, *110*, 210−241.

(2) Holten-Andersen, N.; Waite, J. H. Mussel-Designed Protective Coatings for Compliant Substrates. *J. Dent. Res.* **2008**, *87* (8), 701−709.

(3) Hassenkam, T.; Gutsmann, T.; Hansma, P.; Sagert, J.; Waite, J. H. Giant Bent-Core Mesogens in the Thread Forming Process of Marine Mussels. *Biomacromolecules* **2004**, *5* (4), 1351−1355.

(4) Krauss, S.; Metzger, T. H.; Fratzl, P.; Harrington, M. J. Self-Repair of a Biological Fiber Guided by an Ordered Elastic Framework. *Biomacromolecules* **2013**, *14* (5), 1520−1528.

(5) Taylor, S. W.; Chase, D. B.; Emptage, M. H.; Nelson, M. J.; Waite, J. H. Ferric Ion Complexes of a DOPA-Containing Adhesive




DOI: 10.1021/acs.langmuir.9b01844
*Langmuir* XXXX, XXX, XXX−XXX

Protein From Mytilus Edulis. *Inorg. Chem.* **1996**, *35* (26), 7572−7577.
(6) Harrington, M. J.; Masic, A.; Holten-Andersen, N.; Waite, J. H.; Fratzl, P. Iron-Clad Fibers: a Metal-Based Biological Strategy for Hard Flexible Coatings. *Science* **2010**, *328* (5975), 216−220.
(7) Holten-Andersen, N.; Fantner, G. E.; Hohlbauch, S.; Waite, J. H.; Zok, F. W. Protective Coatings on Extensible Biofibres. *Nat. Mater.* **2007**, *6* (9), 669−672.
(8) Xu, Z. Mechanics of Metal-Catecholate Complexes: the Roles of Coordination State and Metal Types. *Sci. Rep.* **2013**, *3* (1), 216−217.
(9) Cooper, L. H. N. Oxida Tion-Reduction Potential in Sea Water by Cooper, L. H. N. *Ph.D., F.I.C.* DOI: 10.1017/S0025315400011929 2008, 1−10.
(10) Monnier, C. A.; DeMartini, D. G.; Waite, J. H. Intertidal Exposure Favors the Soft-Studded Armor of Adaptive Mussel Coatings. *Nat. Commun.* **2018**, *9*, 1−9.
(11) Priemel, T.; Degtyar, E.; Dean, M. N.; Harrington, M. J. Rapid Self-Assembly of Complex Biomolecular Architectures During Mussel Byssus Biofabrication. *Nat. Commun.* **2017**, *8*, 1−12.
(12) DeMartini, D. G.; Errico, J. M.; Sjoestroem, S.; Fenster, A.; Waite, J. H. A Cohort of New Adhesive Proteins Identified From Transcriptomic Analysis of Mussel Foot Glands. *J. R. Soc., Interface* **2017**, *14* (131), 20170151−14.
(13) Sun, C.; Waite, J. H. Mapping Chemical Gradients Within and Along a Fibrous Structural Tissue, Mussel Byssal Threads. *J. Biol. Chem.* **2005**, *280* (47), 39332−39336.
(14) Hullebusch, E. V.; Rossano, S.; Farges, F.; Lenz, M.; Labanowski, J.; Lagarde, P.; Flank, A.-M.; Lens, P. Sulfur K-Edge XANES Spectroscopy as a Tool for Understanding Sulfur Chemical State in Anaerobic Granular Sludge. *J. Phys.: Conf. Ser.* **2009**, *190*, 012184−012185.
(15) Almkvist, G.; Boye, K.; Persson, I. K-Edge XANES Analysis of Sulfur Compounds: an Investigation of the Relative Intensities Using Internal Calibration. *J. Synchrotron Radiat.* **2010**, *17* (2010), 683−688.
(16) Ray, S.; Shard, A. G. Secondary Ion Mass Spectrometry of Proteins. *International Journal of Physical and Mathmatical Sciences* **2011**, *5* (4), 552−556.
(17) Waite, J. H. Mussel Adhesion - Essential Footwork. *J. Exp. Biol.* **2017**, *220* (4), 517−530.
(18) Li, Y.; Wen, J.; Qin, M.; Cao, Y.; Ma, H.; Wang, W. Single-Molecule Mechanics of Catechol-Iron Coordination Bonds. *ACS Biomater. Sci. Eng.* **2017**, *3* (6), 979−989.
(19) Zeng, H.; Hwang, D. S.; Israelachvili, J. N.; Waite, J. H. Strong Reversible Fe3+-Mediated Bridging Between Dopa-Containing Protein Films in Water. *Proc. Natl. Acad. Sci. U. S. A.* **2010**, *107*, 12850.
(20) Nicklisch, S. C. T.; Waite, J. H. Optimized DPPH Assay in a Detergent-Based Buffer System for Measuring Antioxidant Activity of Proteins. *Methods X* **2014**, *1*, 233−238.
(21) Shimamura, T.; Sumikura, Y.; Yamazaki, T.; Tada, A.; Kashiwagi, T.; Ishikawa, H.; Matsui, T.; Sugimoto, N.; Akiyama, H.; Ukeda, H. Applicability of the DPPH Assay for Evaluating the Antioxidant Capacity of Food Additives - Inter-Laboratory Evaluation Study. *Anal. Sci.* **2014**, *30* (7), 717−721.
(22) Liu, Z.; Meyers, M. A.; Zhang, Z.; Ritchie, R. O. Functional Gradients and Heterogeneities in Biological Materials: Design Principles, Functions, and Bioinspired Applications. *Prog. Mater. Sci.* **2017**, *88*, 467−498.
(23) Moses, D. N.; Mattoni, M. A.; Slack, N. L.; Waite, J. H.; Zok, F. W. Role of Melanin in Mechanical Properties of Glycera Jaws. *Acta Biomater.* **2006**, *2* (5), 521−530.
(24) Poole, L. B. The Basics of Thiols and Cysteines in Redox Biology and Chemistry. *Free Radical Biol. Med.* **2015**, *80*, 148−157.
(25) Nicklisch, S. C. T.; Spahn, J. E.; Zhou, H.; Gruian, C. M.; Waite, J. H. Redox Capacity of an Extracellular Matrix Protein Associated with Adhesion in Mytilus Californianus. *Biochemistry* **2016**, *55* (13), 2022−2030.


DOI: 10.1021/acs.langmuir.9b01844
*Langmuir* XXXX, XXX, XXX−XXX